Nature of Nuclear Non-axiality Seen Through Exotic Geometrical Symmetries: New Concepts of Nuclear Shells

Jerzy DUDEK

Université de Strasbourg et IN_2P_3/CNRS, France

Chirality and Wobbling in Atomic Nuclei
CWAN'23, Huizhou, China

COLLABORATORS

Irene Dedes

IFJ, Polish Academy of Sciences, Cracow, Poland

Andrzej Baran, Andrzej Góźdź and Jie Yang

UMCS, Lublin, Poland

Dominique Curien and David Rouvel

IPHC and University of Strasbourg, France

Rami Gaamouci
IFJ, Polish Academy of Sciences, Cracow, Poland

Mathew Martin, Kris Starosta

Simon Fraser University, Burnaby, British Columbia, Canada

Aleksandra Pędrak

National Centre for Nuclear Research, Warsaw, Poland

Hua-Lei Wang

Zhengzhou University, Zhengzhou, China

The Content of the Present Project

The Content of the Present Project

1) Nuclear Structure Physics Elements:

Realistic Phenomenological Mean-Field Theory,
Nuclear Shapes, Their Symmetries and Quantum Manifestations,
Quantum Rotors with Exotic Symmetries,
Experimental Criteria of Symmetry Identification

The Content of the Present Project

1) Nuclear Structure Physics Elements:

Realistic Phenomenological Mean-Field Theory,
Nuclear Shapes, Their Symmetries and Quantum Manifestations,
Quantum Rotors with Exotic Symmetries,
Experimental Criteria of Symmetry Identification

2) Mathematical-Physics Elements:

– **Inverse Problem Theory (controlling parameter optimisation)**

– **Group-, and Group Representation Theories (symmetries)**

– **Graph Theory (nuclear motion in deformation spaces)**

Partial Source of Input for the Present Project

- *Exotic shape symmetries around the fourfold octupole magic number $N = 136$: Formulation of experimental identification criteria*

  PHYSICAL REVIEW C 105, 034348 (2022)

- *Exotic symmetries as stabilizing factors for superheavy nuclei: Symmetry-oriented generalized concept of nuclear magic numbers*

  PHYSICAL REVIEW C 106, 054314 (2022)

- *Islands of oblate hyperdeformed and superdeformed superheavy nuclei with D_{3h} point group symmetry in competition with other D_{3h} states: "Archipelago" of D_{3h}-symmetry islands*

  PHYSICAL REVIEW C 107, 054304 (2023)

– – – – – – – – – – –

- These texts employ the language of "magic numbers" despite rather historical background of this notion

Part I

Historical Notion of Magic Numbers
Via Separation Energies

From 1963 Nobel Prize to the XXI Century

- **Observe characteristic differences between the nucleonic and electronic separation spectra**

- **The 1963 Nobel Prize for the study of the nuclear effect to M. Göppert-Mayer, J. Jensen and E. Wigner ↔ See: "Shell Model of Nuclei"**

- **In atomic nuclei the highest-j orbital in an N-shell is ejected to the (N-1st)–shell below it**

- **The big gaps at $Z/N = 20, 28, 50, 82, 126$ are confirmed by spin-orbit mean-field coupling**

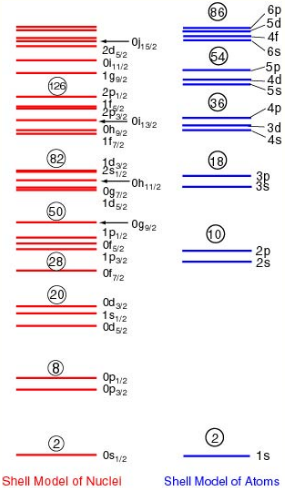

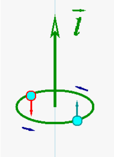

Nuclear Spin-Orbit Splitting – Textbook Version

- **Original from Mayer and Jensen reprinted by Bohr and Mottelson**

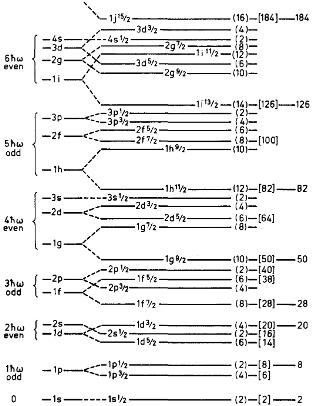

Figure 2-23 Sequence of one-particle orbits. The figure is taken from M. G. Mayer and J. H. D. Jensen, *Elementary Theory of Nuclear Shell Structure*, p. 58, Wiley, New York, 1955.

- **Removing the particles we learn about interactions with the others**
- **A mean-field interaction can be seen as an algorithm probing the two-body interactions through a generalised weighted average $\leftrightarrow \hat{V}$**

$$\hat{V}(\hat{x}) = \frac{1}{N-1} \sum_{j=1}^{(N-1)} \int dx_j \, \psi^*(x_j) \, \hat{V}(\hat{x}, \hat{x}_j) \, \psi(x_j)$$

An N–Body System

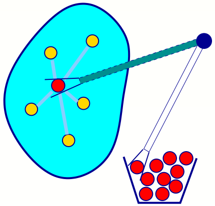

Schematic: Probing 2-body interactions with an 'external' test-particle

- **Removing the particles we learn about interactions with the others**
- **A mean-field interaction can be seen as an algorithm probing the two-body interactions through a generalised weighted average** $\leftrightarrow \widehat{V}$

$$\widehat{V}(\hat{x}) = \frac{1}{N-1} \sum_{j=1}^{(N-1)} \int dx_j \, \psi^*(x_j) \, \widehat{V}(\hat{x}, \hat{x}_j) \, \psi(x_j)$$

- **Observe that summation above implies an averaging over all (N-1) remaining particles**

An N−Body System

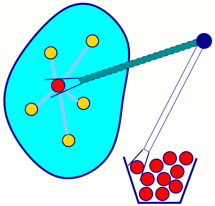

Schematic: Probing 2-body interactions with an 'external' test-particle

- **Removing the particles we learn about interactions with the others**
- **A mean-field interaction can be seen as an algorithm probing the two-body interactions through a generalised weighted average $\leftrightarrow \hat{V}$**

$$\hat{V}(\hat{x}) = \frac{1}{N-1} \sum_{j=1}^{(N-1)} \int dx_j \, \psi^*(x_j) \, \hat{V}(\hat{x}, \hat{x}_j) \, \psi(x_j)$$

- **Observe that summation above implies an averaging over all (N-1) remaining particles**
- **Observe also that the resulting mean-field potential $\hat{V} = \hat{V}(\hat{x})$ is a one-body operator**

An N–Body System

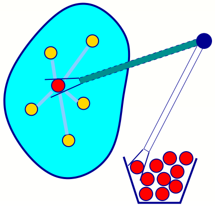

Schematic: Probing 2-body interactions with an 'external' test-particle

- **Removing the particles we learn about interactions with the others**
- **A mean-field interaction can be seen as an algorithm probing the two-body interactions through a generalised weighted average** $\leftrightarrow \hat{V}$

$$\hat{V}(\hat{x}) = \frac{1}{N-1} \sum_{j=1}^{(N-1)} \int dx_j \, \psi^*(x_j) \, \hat{V}(\hat{x}, \hat{x}_j) \, \psi(x_j)$$

- **Observe that summation above implies an averaging over all (N-1) remaining particles**
- **Observe also that the resulting mean-field potential $\hat{V} = \hat{V}(\hat{x})$ is a one-body operator**
- **Right: An artist view of the binding energy experiment as the average interaction tests**

An N−Body System

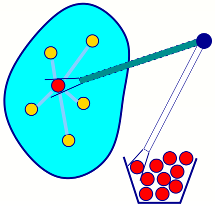

Schematic: Probing 2-body interactions with an 'external' test-particle

- Removing the particles we learn about interactions with the others
- A mean-field interaction can be seen as an algorithm probing the two-body interactions through a generalised weighted average $\leftrightarrow \hat{V}$

$$\hat{V}(\hat{x}) = \frac{1}{N-1} \sum_{j=1}^{(N-1)} \int dx_j \, \psi^*(x_j) \, \hat{V}(\hat{x}, \hat{x}_j) \, \psi(x_j)$$

- Observe that summation above implies an averaging over all (N-1) remaining particles
- Observe also that the resulting mean-field potential $\hat{V} = \hat{V}(\hat{x})$ is a one-body operator
- Right: An artist view of the binding energy experiment as the average interaction tests
- The mean field potential binding non-interacting nucleons $\rightarrow$ is a simple container

An N–Body System

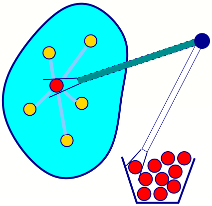

Schematic: Probing 2-body interactions with an 'external' test-particle

There exist powerfull Mean–Field Theories

Hartree–Fock | **Relativistic (RMF)** | **Phenomenological**

↓ ↓ ↓

Ground–State– and Shape–Coexisting Masses

Part II

Mean-Field Approach Selected for This Project:

Realistic Phenomenological (Woods-Saxon) Mean-Field

Description of Nuclear Deformation [or Shapes]

• Given nuclear surface, Σ. It can generally be expanded in terms of spherical harmonics $\{Y_{\lambda\mu}(\theta,\phi)\}$ with complex coefficients $\{\alpha_{\lambda\mu}\}$

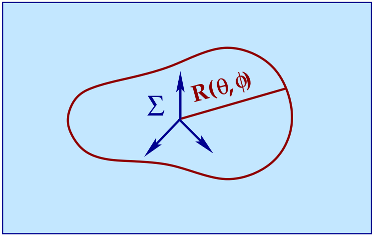

• The formal expansion [standard form]:

$$R(\theta,\phi) \sim R_o\Big[1+\sum_{\lambda\mu}\alpha_{\lambda\mu}Y_{\lambda\mu}(\theta,\phi)\Big];$$

= a multipole expansion about the sphere

• Parameters $\{\alpha_{\lambda\mu}\}$, are usually called *deformations* or shape degrees of freedom

The lowest rank deformations:

$\rightarrow$ $\alpha_{2\mu}$ - quadrupole
$\rightarrow$ $\alpha_{3\mu}$ - octupole
$\rightarrow$ $\alpha_{4\mu}$ - hexadecapole

• For the time-dependent description e.g., collective vibrations or rotations:

$$\boxed{\alpha_{\lambda\mu}=\alpha_{\lambda\mu}(t)}$$

W-S Mean-Field is a Functional of $\mathrm{dist}_\Sigma(\vec{r})$

Given surface Σ

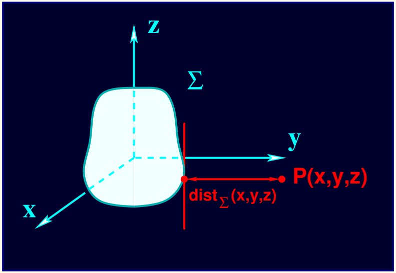

Constructing distance function

Phenomenological Woods-Saxon potential respects automatically the symmetries of the underlying surface Σ:

$$\hat{V}^{\mathrm{WS}}_{\mathrm{Cent}}(\vec{r}) \equiv \frac{V_0}{1+\exp\{\mathrm{dist}_\Sigma(\vec{r})/a\}}$$

$$\hat{V}^{\mathrm{WS}}_{\mathrm{S-O}}(\vec{r}) \equiv \left[\nabla V^{\mathrm{WS}}_{\mathrm{Cent}}(\vec{r}) \wedge \hat{p}\right] \cdot \vec{s}$$

$$\boxed{\hat{V}_{\mathrm{mf}} = \hat{V}^{\mathrm{WS}}_{\mathrm{Cent}} + \hat{V}^{\mathrm{WS}}_{\mathrm{S-O}} + \hat{V}_{\mathrm{C}}}$$

Surface Σ : $\quad R(\vartheta,\varphi) = R_o\, c(\{\alpha\}) \left[1+\sum_\lambda \sum_{\mu=-\lambda}^{\lambda} \alpha_{\lambda}{}^{\mu}\, Y_{\lambda\mu}(\vartheta,\varphi)\right]$

Hamiltonian: $\boxed{\hat{H}_{\mathrm{m-f}} = \hat{T} + \hat{V}_{\mathrm{m-f}}}$

- More precisely, we have 3 parameters for the central potential

$$\hat{\mathcal{V}}^{WS}_{\rm Cent}(\vec{r},\alpha;V^c,r^c,a^c)=\frac{V^c}{1+\exp[{\rm dist}_\Sigma(\vec{r},r^c;\alpha)/a^c]},\;\leftrightarrow\;\frac{V^c}{1+\exp[(r-R^c)/a^c]},$$

- More precisely, we have 3 parameters for the central potential

$$\hat{\mathcal{V}}^{WS}_{\rm Cent}(\vec{r},\alpha; V^c, r^c, a^c) = \frac{V^c}{1+\exp[{\rm dist}_\Sigma(\vec{r}, r^c;\alpha)/a^c]}, \leftrightarrow \frac{V^c}{1+\exp[(r-R^c)/a^c]},$$

and 3 parameters for the spin-orbit potential

$$\hat{\mathcal{V}}^{so}_{WS}(\vec{r},\hat{p},\hat{s},\alpha;\lambda^{so}, r^{so}, a^{so}) = \frac{2\,\hbar c^2}{(2m^*)^2}[(\vec{\nabla} V^{so}_{WS})\wedge \hat{p}]\cdot\hat{s},$$

where

$$V^{so}_{WS}(r,\alpha;\lambda^{so}, r^{so}, a^{so}) = \frac{\lambda^{so}}{1+\exp[{\rm dist}_\Sigma(\vec{r}, r^{so};\alpha)/a^{so}]},$$

= =

- More precisely, we have 3 parameters for the central potential

$$\hat{\mathcal{V}}^{WS}_{\mathrm{Cent}}(\vec{r},\alpha;V^c,r^c,a^c)=\frac{V^c}{1+\exp[\mathrm{dist}_\Sigma(\vec{r},r^c;\alpha)/a^c]},\;\leftrightarrow\;\frac{V^c}{1+\exp[(r-R^c)/a^c]},$$

and 3 parameters for the spin-orbit potential

$$\hat{\mathcal{V}}^{so}_{WS}(\vec{r},\hat{p},\hat{s},\alpha;\lambda^{so},r^{so},a^{so})=\frac{2\,\hbar c^2}{(2m^*)^2}[(\vec{\nabla}V^{so}_{WS})\wedge\hat{p}]\cdot\hat{s},$$

where

$$V^{so}_{WS}(r,\alpha;\lambda^{so},r^{so},a^{so})=\frac{\lambda^{so}}{1+\exp[\mathrm{dist}_\Sigma(\vec{r},r^{so};\alpha)/a^{so}]},$$

= =

- **Our Hamiltonian formally depends on the two sets of 6 parameters each,**

$$\boxed{\{V^c,r^c,a^c,\lambda^{so},r^{so},a^{so}\}_{\pi,\nu}}$$

- **They are fitted to experimental values of single-nucleon level-energies in**

$$\boxed{{}^{16}\mathrm{O},\ {}^{40}\mathrm{Ca},\ {}^{48}\mathrm{Ca},\ {}^{56}\mathrm{Ni},\ {}^{90}\mathrm{Zr},\ {}^{132}\mathrm{Sn},\ {}^{146}\mathrm{Gd},\ {}^{208}\mathrm{Pb}}$$

• Attention: χ^2-fitting is just the beginning; it must be accompanied by a number of operations assuring a minimum of stochastic sense

• Attention: χ^2-fitting is just the beginning; it must be accompanied by a number of operations assuring a minimum of stochastic sense

About the So-Called Chi-By-the-Eye "Method"

• In their introduction to the book chapter *'Modelling of Data'*, the authors of *'Numerical Recipes*" (p. 651), observe with sarcasm:

• Attention: χ^2-fitting is just the beginning; it must be accompanied by a number of operations assuring a minimum of stochastic sense

About the So-Called Chi-By-the-Eye "Method"

• In their introduction to the book chapter *'Modelling of Data'*, the authors of *'Numerical Recipes*" (p. 651), observe with sarcasm:

"Unfortunately, many practitioners of parameter estimation never proceed beyond determining the numerical values of the parameter fit. They deem a fit acceptable if a graph of data and model ' l o o k s   g o o d '. This approach is known as chi-by-the-eye. Luckily, its practitioners get what they deserve" [what is meant is: "they" obtain a 'meaningless result']

• Attention: χ^2-fitting is just the beginning; it must be accompanied by a number of operations assuring a minimum of stochastic sense

About the So-Called Chi-By-the-Eye "Method"

• In their introduction to the book chapter *'Modelling of Data'*, the authors of *'Numerical Recipes"* (p. 651), observe with sarcasm:

"Unfortunately, many practitioners of parameter estimation never proceed beyond determining the numerical values of the parameter fit. They deem a fit acceptable if a graph of data and model ' l o o k s   g o o d '. This approach is known as chi-by-the-eye. Luckily, its practitioners get what they deserve" [what is meant is: "they" obtain a 'meaningless result']

Meaningless result ← less politely → Equivalent to random numbers

- **One demonstrates within Inverse Problem Theory an importance of removal of parameter correlations**

- **One demonstrates within Inverse Problem Theory an importance of removal of parameter correlations**

- **We determine the existence and remove parameter correlations employing Monte-Carlo simulations *)**

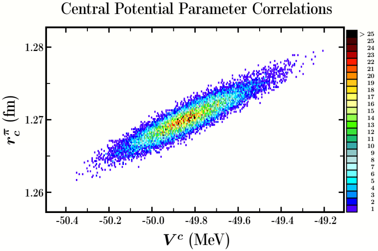

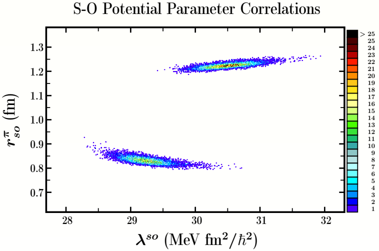

***) See PHYSICAL REVIEW C 103, 054311 (2021) and references therein**

- **Parametric correlations present**

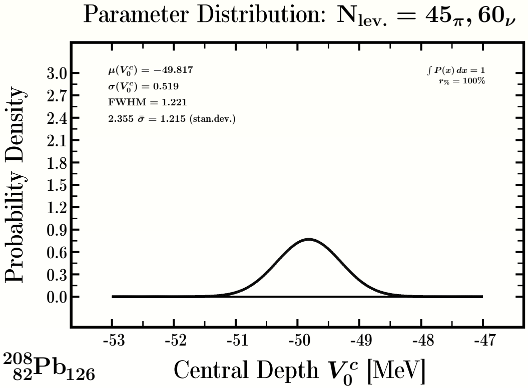

Probability of Uncertainty. Here: Central potential depth, V_0^c, for Woods-Saxon Universal

- **Parametric correlations removed**

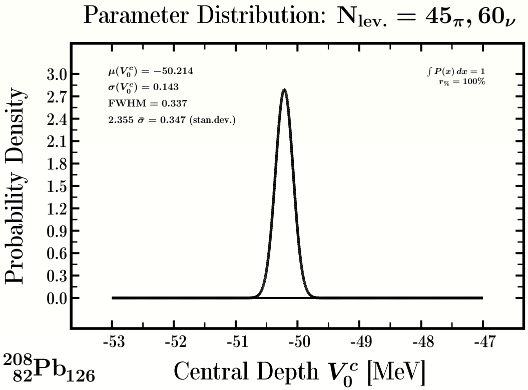

Probability of Uncertainty. Here: Central potential depth, V_0^c, for Woods-Saxon Universal

- **Parametric correlations present**

Parameter Distribution: $\mathbf{N_{lev.} = 45_\pi, 60_\nu}$

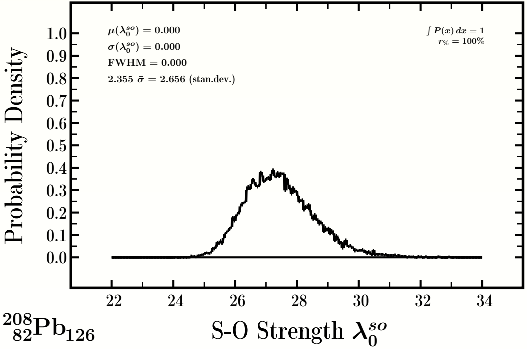

$^{208}_{82}\mathrm{Pb}_{126}$

Probability of Uncertainty. Here: spin-orbit potential strength, λ_0^{so}, for Woods-Saxon Universal

- **Parametric correlations removed**

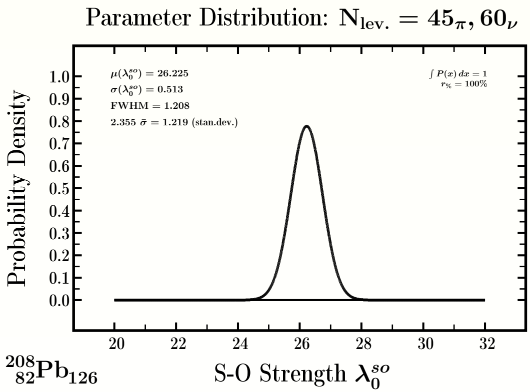

Probability of Uncertainty. Here: spin-orbit potential strength, λ_0^{so}, for Woods-Saxon Universal

Consequences for Our Project

- Our total energy calculations are performed using the Hamiltonian parametrisation with parametric correlations removed

Consequences for Our Project

• Our total energy calculations are performed using the Hamiltonian parametrisation with parametric correlations removed

• According to Inverse Problem Theory this assures maximum stochastic stability of modelling predictions

Part III

Contemporary View of Octupole 'Magic Numbers' Through Phenomenological Realistic Mean Field Hamiltonian

Below we present selected results about: 4-Fold Octupole Magic Number N = 136

PHYSICAL REVIEW C **105**, 034348 (2022)

Exotic shape symmetries around the fourfold octupole magic number $N = 136$: Formulation of experimental identification criteria

J. Yang,[1,2] J. Dudek,[3,*] I. Dedes,[4] A. Baran,[2] D. Curien,[3] A. Gaamouci,[5] A. Góźdź,[2] A. Pędrak,[6] D. Rouvel,[3] H. L. Wang,[1] and J. Burkat[7]

[1]*School of Physics and Microelectronics, Zhengzhou University, Zhengzhou 450001, China*
[2]*Institute of Physics, Marie Curie-Skłodowska University, PL-20 031 Lublin, Poland*
[3]*Université de Strasbourg, CNRS, IPHC UMR 7178, F-67 000 Strasbourg, France*
[4]*Institute of Nuclear Physics, Polish Academy of Sciences, PL-31 342 Kraków, Poland*
[5]*Laboratoire de Physique Théorique, Faculté de Physique, USTHB, BP 32, El Alia, 16111 Bab Ezzouar, Algiers, Algeria*
[6]*National Centre for Nuclear Research, Theoretical Physics Division, Pl-02-093 Warsaw, Poland*
[7]*Brasenose College, University of Oxford, Oxford OX1 4AJ, United Kingdom*

(Received 1 February 2022; accepted 21 March 2022; published 31 March 2022)

- Mean-field $\hat{Q}_{\lambda=3}$ repulsion between $2g_{9/2}$ and $1j_{15/2}$ neutron orbitals

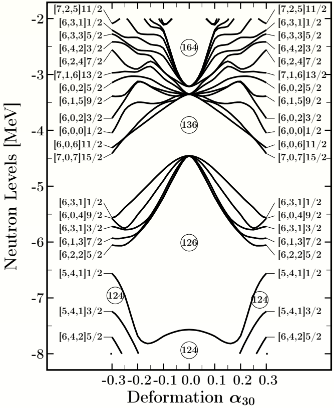

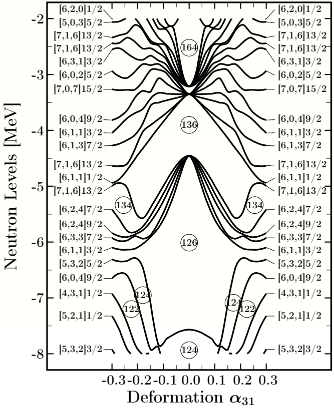

- **Notice octupole $N = 136$ shell gap above spherical $N = 126$ shell gap**

Octupole 4-Fold Magic Number N = 136: Follow with (α_{32} and α_{33})

- Mean-field $\hat{Q}_{\lambda=3}$ repulsion between $2g_{9/2}$ and $1j_{15/2}$ neutron orbitals

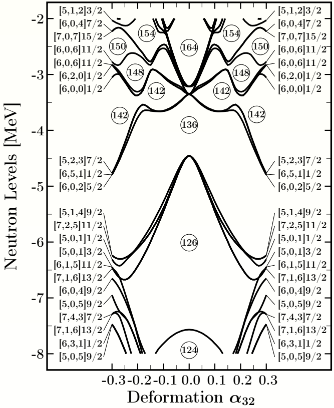

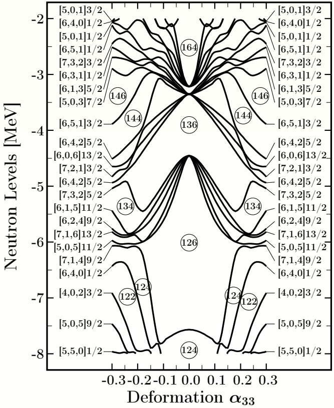

- **Notice octupole $N = 136$ shell gap above spherical $N = 126$ shell gap**

To emphasise: Tetrahedral symmetry gap α_{32} almost as large as $N = 126$

Comments: Why 4-Fold Magic number?

- **Observe that in contrast to the traditional magic numbers applying to spherical symmetry – the octupole magic numbers "remain magic and the same" for four different symmetries**

Comments: Why 4-Fold Magic number?

• Observe that in contrast to the traditional magic numbers applying to spherical symmetry – the octupole magic numbers "remain magic and the same" for four different symmetries

• Thanks to the octupole 4-fold magic number $N = 136$, the multipoles $\lambda = 3$ (octupole) rather than $\lambda = 2$ (quadrupole) introduce non-sphericity $\leftrightarrow$ exotic deformations & symmetries

Pb Looses Sphericity for $N = 130, 134, \ldots$ Because of $\alpha_{3\mu}$ and NOT $\alpha_{2\mu}$

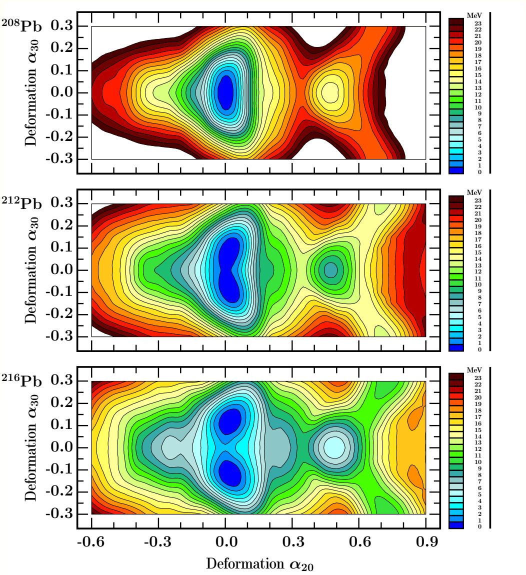

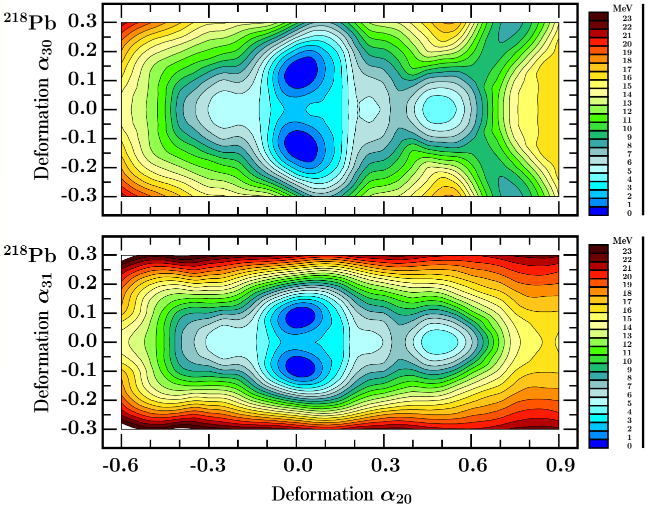

- **Note the predicted octupole (not quadrupole) non-sphericity: ^{218}Pb$_{136}$**

- Large barriers, over 3 MeV, separating double tetrahedral minima

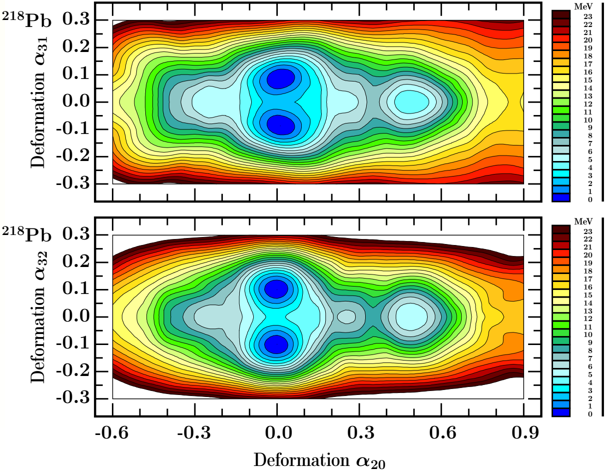

- **Note the predicted octupole (not quadrupole) non-sphericity: ^{218}Pb$_{136}$**

- Large barriers, over 3 MeV, separating double tetrahedral minima

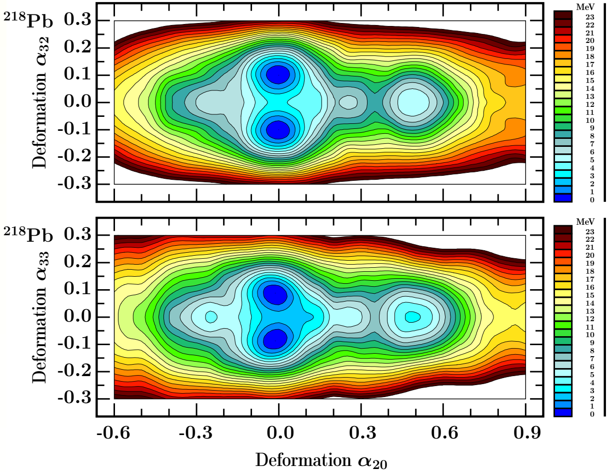

- **Note the predicted octupole (not quadrupole) non-sphericity: $^{218}Pb_{136}$**

Good News When Looking for Exotic Symmetries!!

• **In this project Exotic Symmetries are defined as anything but ellipsoidal $(\alpha_{20}, \alpha_{22})$ or pear-shape $(\alpha_{20}, \alpha_{30})$**

• **Emphasise that often a polarisation of a doubly-magic nucleus by**

$$(N_0, Z_0) \to (N_0 \pm \Delta N, Z_0 \pm \Delta Z)$$

leads to prolate/oblate/ellipsoidal deformations – thus "not for us"

Good News When Looking for Exotic Symmetries!!

• **In this project Exotic Symmetries are defined as anything but ellipsoidal (α_{20}, α_{22}) or pear-shape (α_{20}, α_{30})**

• **Emphasise that often a polarisation of a doubly-magic nucleus by**
$$(N_0, Z_0) \to (N_0 \pm \Delta N, Z_0 \pm \Delta Z)$$
leads to prolate/oblate/ellipsoidal deformations – thus "not for us"

• **Thanks to the octupole 4-fold $N = 136$ magic number multipoles $\lambda = 3$ (octupole) rather than $\alpha_{\lambda=2}$ (quadrupole) introduce the sought exotic deformations & symmetries**

Good News When Looking for Exotic Symmetries!!

- **In this project Exotic Symmetries are defined as anything but ellipsoidal (α_{20}, α_{22}) or pear-shape (α_{20}, α_{30})**

- **Emphasise that often a polarisation of a doubly-magic nucleus by**

$$(N_0, Z_0) \to (N_0 \pm \Delta N, Z_0 \pm \Delta Z)$$

leads to prolate/oblate/ellipsoidal deformations – thus "not for us"

- **Thanks to the octupole 4-fold $N = 136$ magic number multipoles $\lambda = 3$ (octupole) rather than $\alpha_{\lambda=2}$ (quadrupole) introduce the sought exotic deformations & symmetries**

- **Therefore thanks to the leading role of $\alpha_{\lambda=3,\mu}$ multipoles $\to$ We arrive at the "mine of exotic (molecular) symmetries"**

Good News When Looking for Exotic Symmetries!!

• In this project **Exotic Symmetries** are defined as anything but ellipsoidal $(\alpha_{20}, \alpha_{22})$ or pear-shape $(\alpha_{20}, \alpha_{30})$

• Emphasise that often a polarisation of a doubly-magic nucleus by

$$(N_0, Z_0) \rightarrow (N_0 \pm \Delta N, Z_0 \pm \Delta Z)$$

leads to prolate/oblate/ellipsoidal deformations – thus **"not for us"**

• Thanks to the octupole 4-fold $N = 136$ magic number multipoles $\lambda = 3$ (octupole) rather than $\alpha_{\lambda=2}$ (quadrupole) introduce the sought **exotic deformations & symmetries**

• Therefore thanks to the leading role of $\alpha_{\lambda=3,\mu}$ multipoles
$\rightarrow$ We arrive at the **"mine of exotic (molecular) symmetries"**

What are these exotic molecular symmetries?

- **Symmetry induced by both $\alpha_{31} \neq 0$ and $(\alpha_{20} \neq 0, \alpha_{31} \neq 0)$**

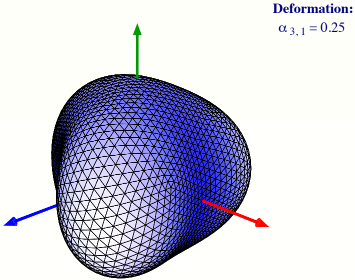

$\alpha_{31} = 0.25$

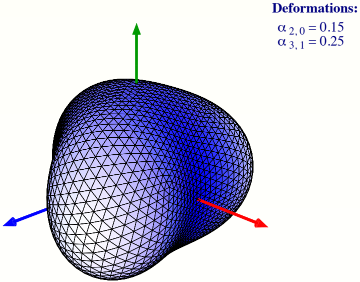

$\alpha_{20} = 0.15, \alpha_{31} = 0.25$

Nuclear C_{2v} Point Group Symmetry

- **Symmetry induced by both $\alpha_{33} \neq 0$ and $(\alpha_{20} \neq 0, \alpha_{33} \neq 0)$**

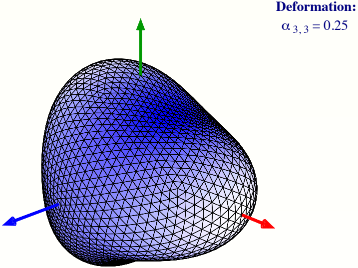

$\alpha_{33} = 0.25$

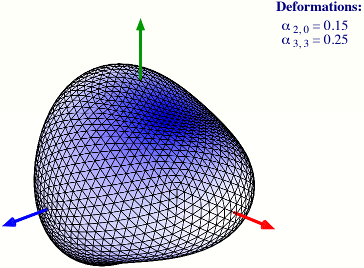

$\alpha_{20} = 0.15, \alpha_{33} = 0.25$

Nuclear D_{3h} Point Group Symmetry

- **Symmetry induced by $\alpha_{32} \neq 0$ and $(\alpha_{20} \neq 0, \alpha_{32} \neq 0)$**

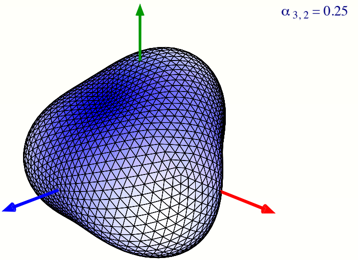

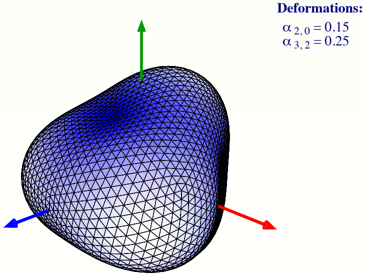

Tetrahedral T_d: $\alpha_{32} = 0.25$

D_{2d}: $\alpha_{20} = 0.15, \alpha_{32} = 0.25$

Nuclear T_d and D_{2d} Point Group Symmetries

Having introduced exotic symmetries:

Let us enter what we call

New Spectroscopy: Issues & Challenges

Rotating High-Rank Symmetric Nuclei
Seen Through Group-Representation Theory

[Example: Tetrahedral Symmetry Quantum Rotors]

Remarks for theorists / not essential for discussing conclusions →

- Let G be the symmetry group of the quantum rotor Hamiltonian
- Let $\{D_i,\ i = 1, 2, \ldots M\}$ be the irreducible representations of G
- The representation $D^{(I\pi)}$ of the rotor states with the definite spin-parity $I\pi$, can be decomposed in terms of D_i with multiplicities $a_i^{(I\pi)}$:

$$\boldsymbol{D^{(I\pi)} = \sum_{i=1}^{M} a_i^{(I\pi)} D_i}$$

- Multiplicities [M. Hamermesh, *Group Theory*, 1962] are given by:

$$\boldsymbol{a_i^{(I\pi)} = \frac{1}{N_G} \sum_{R \in G} \chi_{I\pi}(R) \chi_i(R) = \frac{1}{N_G} \sum_{\alpha=1}^{M} g_\alpha \chi_{I\pi}(R_\alpha) \chi_i(R_\alpha);}$$

N_G: order of the group G; $\{\chi_{I\pi}(R), \chi_i(R)\}$: characters of $\{D^{(I\pi)}, D_i\}$
R: group element; g_α: the number of elements in the class α, whose representative element is R_α.

- Tetrahedral group has 5 irreducible representations and 5 classes
- The representative elements $\{R\}$ are: $E,\ C_2\,(=S_4^2),\ C_3,\ \sigma_d,\ S_4$
- The characters of irreducible representation of T_d are listed below

T_d	E	$C_3(8)$	$C_2(3)$	$\sigma_d(2)$	$S_4(6)$
A_1	1	1	1	1	1
A_2	1	1	1	−1	−1
E	2	−1	2	0	0
$F_1(T_1)$	3	0	−1	−1	1
$F_2(T_2)$	3	0	−1	1	−1

- The characters $\chi_{I\pi}(R_\alpha)$ for the rotor representations are as follows:

$$\chi_{I\pi}(E)=2I+1,\ \chi_{I\pi}(C_n)=\sum_{K=-I}^{I} e^{\frac{2\pi K}{n}i},\ \chi_{I\pi}(\sigma_d)=\pi\times\chi_{I\pi}(C_2),\ \chi_{I\pi}(S_4)=\pi\times\chi_{I\pi}(C_4)$$

- From these relations we obtain ‘employing the pocket calculator’:

$$a_i^{(I\pi)}=\frac{1}{N_G}\sum_{\alpha=1}^{M} g_\alpha\chi_{I\pi}(R_\alpha)\chi_i(R_\alpha)\ \leftrightarrow\ a_{A_1}^{(I\pm)}=a_{A_2}^{(I\mp)},\ a_E^{(I+)}=a_E^{(I-)},\ a_{F_1}^{(I\pm)}=a_{F_2}^{(I\mp)}$$

- The number of states $a_i^{(I\pi)}$ within five irreducible representations.

If $a_i^{(I\pi)} = 0 \;\rightarrow$ states not allowed; $a_i^{(I\pi)} = 2 \;\rightarrow$ doubly degenerate

I^+	0^+	1^+	2^+	3^+	4^+	5^+	6^+	7^+	8^+	9^+	10^+
A_1	1	0	0	0	1	0	1	0	1	1	1
A_2	0	0	0	1	0	0	1	1	0	1	1
E	0	0	1	0	1	1	1	1	2	1	2
$F_1(T_1)$	0	1	0	1	1	2	1	2	2	3	2
$F_2(T_2)$	0	0	1	1	1	1	2	2	2	2	3

I^-	0^-	1^-	2^-	3^-	4^-	5^-	6^-	7^-	8^-	9^-	10^-
A_1	0	0	0	1	0	0	1	1	0	1	1
A_2	1	0	0	0	1	0	1	0	1	1	1
E	0	0	1	0	1	1	1	1	2	1	2
$F_1(T_1)$	0	0	1	1	1	1	2	2	2	2	3
$F_2(T_2)$	0	1	0	1	1	2	1	2	2	3	2

- In this way we find the spin-parity sequence for A_1-representation

$$\mathrm{A_1}: \quad 0^+, 3^-, 4^+, 6^+, 6^-, 7^-, 8^+, 9^+, 9^-, 10^+, 10^-, 11^-, 2\times 12^+, 12^-, \cdots$$

Concluding: 'Take Home' Message

The bottom line for an experimentalist:

The tetrahedral ground-state band $I^\pi = 0^+$ is composed of the following states:

$$\mathbf{A_1:}\quad \mathbf{0^+,\, 3^-,\, 4^+,\, 6^+,\, 6^-,\, 7^-,\, 8^+,\, 9^+,\, 9^-,\, 10^+,\, 10^-,\, 11^-,\, 2\times 12^+,\, 12^-,\, \cdots}$$

The bottom line for an experimentalist:

The tetrahedral ground-state band $I^\pi = 0^+$ is composed of the following states:

$$\mathbf{A_1}: \quad 0^+, 3^-, 4^+, 6^+, 6^-, 7^-, 8^+, 9^+, 9^-, 10^+, 10^-, 11^-, 2\times 12^+, 12^-, \cdots$$

Its structure has not much in common with the “usual” one(s), e.g.:

$$I^\pi = 0^+, 2^+, 4^+, \ \ldots$$

and implies a new way of thinking (and acting)

This Group Theory Result Is Obtained Directly by HFB Angular Momentum and Parity Projection

PHYSICAL REVIEW C **87**, 054306 (2013)

Microscopic study of tetrahedrally symmetric nuclei by an angular-momentum and parity projection method

Shingo Tagami and Yoshifumi R. Shimizu
Department of Physics, Faculty of Sciences, Kyushu University, Fukuoka 812-8581, Japan

Jerzy Dudek
Institut Pluridisciplinaire Hubert Curien (IPHC), IN_2P_3-CNRS/Université de Strasbourg, F-67037 Strasbourg, France
(Received 9 January 2013; revised manuscript received 4 March 2013; published 7 May 2013)

We study the properties of the nuclear rotational excitations with hypothetical tetrahedral symmetry by employing the microscopic mean-field and residual-interaction Hamiltonians with angular-momentum and parity projection method; we focus on the deformed nuclei with tetrahedral doubly closed shell configurations. We find that for pure tetrahedral deformation the obtained excitation patterns satisfy the characteristic features predicted by group-representation theory applied to the tetrahedral symmetry group. We find that a gradual transition from the approximately linear to the characteristic rigid-rotor, parabolic energy-vs.-spin dependence occurs as a function of the tetrahedral deformation parameter. The form of this transition is compared with the similar well-known transition in the case of quadrupole deformation.

This Group Theory Result Is Obtained Directly by HFB Angular Momentum and Parity Projection

SHINGO TAGAMI, YOSHIFUMI R. SHIMIZU, AND JERZY DUDEK PHYSICAL REVIEW C **87**, 054306 (2013)

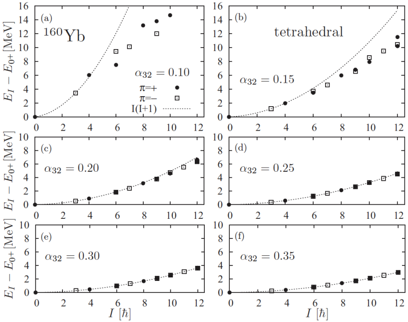

FIG. 4. Calculated spectra of tetrahedral states in ^{160}Yb with $\alpha_{32} = 0.10, 0.15, 0.20, 0.25, 0.30$, and 0.35, respectively, for (a), (b), (c), (d), (e), and (f). The dotted line in each panel denotes an ideal $I(I+1)$ sequence going through the first excited 3^- state. Note that almost exact degeneracies for $I = (6^+, 6^-), (9^+, 9^-), (10^+, 10^-), (2 \times 12^+, 12^-)$ states are obtained for $\alpha_{32} \geqslant 0.25$ demonstrating the nearly perfect rotor character of the rotational excitation of the system.

Next Steps in the Procedure: Identifying T_d Symmetry

We Proceed Looking for Experimental Candidate States

Criterion no. 1:
We have demonstrated that collective E1 or E2 transitions are forbidden in the tetrahedral symmetry limit $\rightarrow$ may lead to isomers

Criterion no. 2:
Accepted states must neither be populated nor depopulated by any strong E1 or E2 transitions, preferably populated by nuclear reaction

Criterion No. 3:
Their energies should be 'reasonably' close to the reference parabola

Observation:
Since they do not decay via a single strong transition it is instructive verifying that they decay into several states – with weak intensities

Next Steps in the Procedure: Part 2

A typical diagram among a hundred in this analysis

Feedig the tetrahedral $I^{\pi} = 3^{-}$ candidate (among five others)

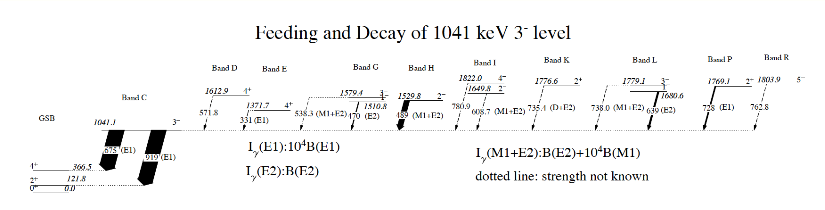

Let us note that 3^{-} does not decay to the 0^{+} ground-states (suggesting that it is not an octuple vibrational state built on the other) and that there are numerous states populating it suggesting that its structure is exotic from our point of view.

[By the way, this state was not retained at the final steps]

Next Steps in the Procedure: Part 2

A typical diagram among a hundred in this analysis

Decay from the tetrahedral $I^{\pi} = 3^{-}$ candidate (among five others)

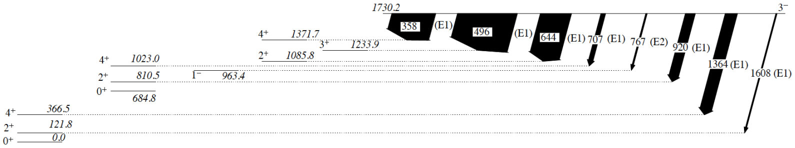

Let us observe that this state decays to many others suggesting its 'exotic' structure of interest in our context

Next Steps in the Procedure: Part 2

A typical diagram among a hundred in this analysis

Decay from the tetrahedral $I^{\pi} = 4^{+}$ candidate level

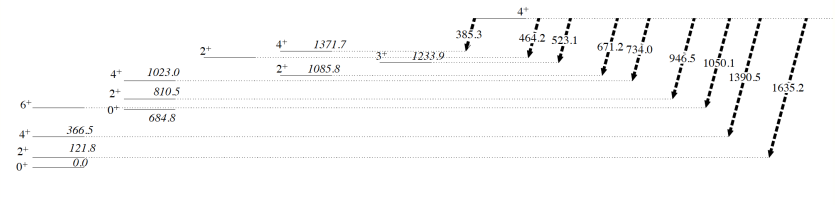

Let us observe that this state decays to many others via very weak transitions suggesting no resemblance to quadrupole-deformed rotational states...

and many, many other states analysed within this project...

Another Example of the Spectra To Test Criteria

- **We must try to find the sequence which is parabolic, no E2 transitions**

$$4^+,\ 6^+,\ 8^+,\ 10^+\ \ldots$$

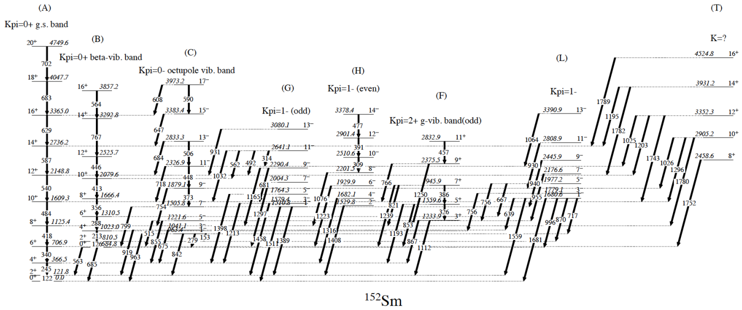

Experimental spectrum of ^{152}Sm

By the way, band (T) was NOT retained in the final analysis

Part III

About the Experimental Evidence*)

for the First Tetrahedral Rotor Case: ^{152}Sm

*) J. Dudek, D. Curien, I. Dedes, K. Mazurek, S. Tagami, Y. R. Shimizu and T. Bhattacharjee; PHYSICAL REVIEW C 97, 021302(R) (2018)

Quantum Rotors: Tetrahedral vs. Octahedral

- The tetrahedral symmetry group has 5 irreducible representations
- The ground-state $I^\pi = 0^+$ belongs to A_1 representation given by:

$$\underbrace{\mathrm{A}_1: \quad 0^+, 3^-, 4^+, \underbrace{(6^+, 6^-)}_{\text{doublet}}, 7^-, 8^+, \underbrace{(9^+, 9^-)}_{\text{doublet}}, \underbrace{(10^+, 10^-)}_{\text{doublet}}, 11^-, \underbrace{2\times 12^+, 12^-}_{\text{triplet}}, \cdots}_{\textbf{Forming a common parabola}}$$

- There are no states with spins $I = 1, 2$ and 5. We have parity doublets: $I = 6, 9, 10 \ldots$, at energies: $E_{6^-} = E_{6^+}$, $E_{9^-} = E_{9^+}$, etc.

Quantum Rotors: Tetrahedral vs. Octahedral

- The tetrahedral symmetry group has 5 irreducible representations
- The ground-state $I^\pi = 0^+$ belongs to A_1 representation given by:

$$\underbrace{\mathrm{A}_1: \quad 0^+,\, 3^-,\, 4^+,\, \underbrace{(6^+, 6^-)}_{\text{doublet}},\, 7^-,\, 8^+,\, \underbrace{(9^+, 9^-)}_{\text{doublet}},\, \underbrace{(10^+, 10^-)}_{\text{doublet}},\, 11^-,\, \underbrace{2\times 12^+,\, 12^-}_{\text{triplet}},\, \cdots}_{\textbf{Forming a common parabola}}$$

- There are no states with spins $I = 1, 2$ and 5. We have parity doublets: $I = 6, 9, 10 \ldots$, at energies: $E_{6^-} = E_{6^+}$, $E_{9^-} = E_{9^+}$, etc.

- One shows that the analogue structure in the octahedral symmetry

$$\underbrace{A_{1g}:\; 0^+, 4^+, 6^+, 8^+, 9^+, 10^+, \;\ldots,\;\; I^\pi = I^+}_{\textbf{Forming a common parabola}}$$

$$\underbrace{A_{2u}:\; 3^-, 6^-, 7^-, 9^-, 10^-, 11^-, \ldots,\;\; I^\pi = I^-}_{\textbf{Forming another (common) parabola}}$$

Quantum Rotors: Tetrahedral vs. Octahedral

- The tetrahedral symmetry group has 5 irreducible representations
- The ground-state $I^\pi = 0^+$ belongs to A_1 representation given by:

$$\underbrace{\mathrm{A}_1 : \quad 0^+, 3^-, 4^+, \underbrace{(6^+, 6^-)}_{\text{doublet}}, 7^-, 8^+, \underbrace{(9^+, 9^-)}_{\text{doublet}}, \underbrace{(10^+, 10^-)}_{\text{doublet}}, 11^-, \underbrace{2\times 12^+, 12^-}_{\text{triplet}}, \cdots}_{\textbf{Forming a common parabola}}$$

- There are no states with spins $I = 1, 2$ and 5. We have parity doublets: $I = 6, 9, 10 \ldots$, at energies: $E_{6^-} = E_{6^+}$, $E_{9^-} = E_{9^+}$, etc.

- One shows that the analogue structure in the octahedral symmetry

$$\underbrace{A_{1g} : \; 0^+, 4^+, 6^+, 8^+, 9^+, 10^+, \; \ldots, \; I^\pi = I^+}_{\textbf{Forming a common parabola}}$$

$$\underbrace{A_{2u} : \; 3^-, 6^-, 7^-, 9^-, 10^-, 11^-, \ldots, \; I^\pi = I^-}_{\textbf{Forming another (common) parabola}}$$

Consequently we should expect two independent parabolic structures

Dominating Tetrahedral-Symmetry Hypothesis

Experimental Results [T_d -*vs.*-O_h]

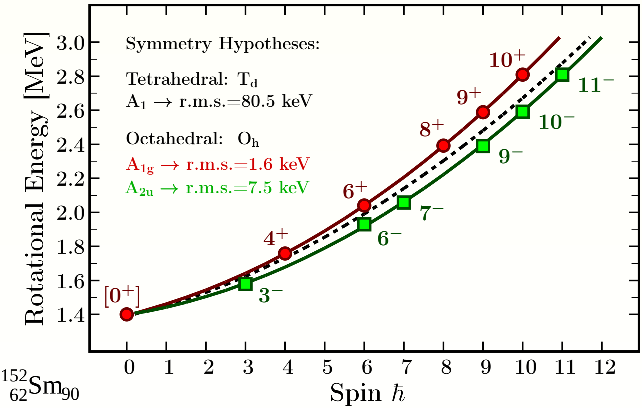

Graphical representation of the experimental data from the summary Table. Curves represent the fit and are *not* meant 'to guide the eye'. Markedly, point [$I^\pi = 0^+$], is a prediction by extrapolation - not an experimental datum.

- **These two sequences represent the coexistence between tetrahedral and octahedral symmetries. Curves represent the parabolas – and are not meant to guide the eye. This is the first evidence based on the experimental data**

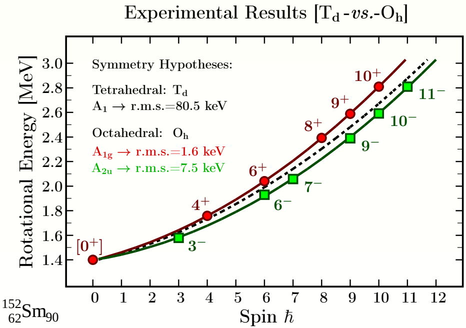

FROM: **Spectroscopic criteria for identification of nuclear tetrahedral and octahedral symmetries: Illustration on a rare earth nucleus**

J. Dudek et al., PHYSICAL REVIEW C 97, 021302(R) (2018)

Those Are Predicted to Contain Long Life Isomers

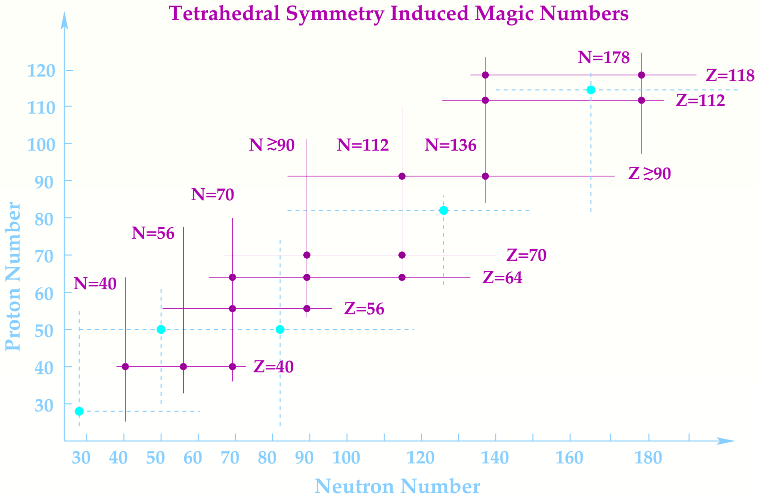

Those Are Predicted to Contain Long Life Isomers

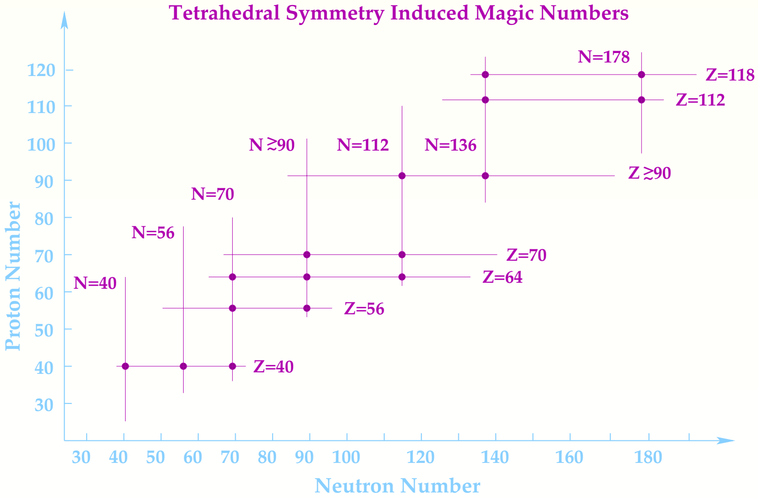

• If you work on exotic nuclei and wish to save millions measuring long-lived isomers rather than short lived ground states – please join

Part IV

Quantum Rotors

carrying other Point Group Symmetries

will be treated in full analogy

The first tetrahedral symmetry evidence based on the experimental data

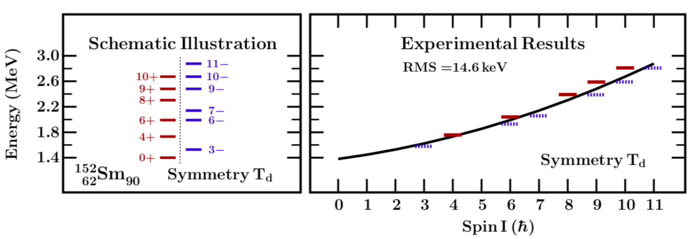

Tetrahedral Band : $I^{\pi}_{T_d} = 0^+, 3^-, 4^+, 6^{\pm}, 7^-, 8^+, 9^{\pm}, 10^{\pm}, 11^-, \ldots$

→ **Published in: J. Dudek et al., PHYSICAL REVIEW C 97, 021302(R) (2018)**

The first tetrahedral symmetry evidence based on the experimental data

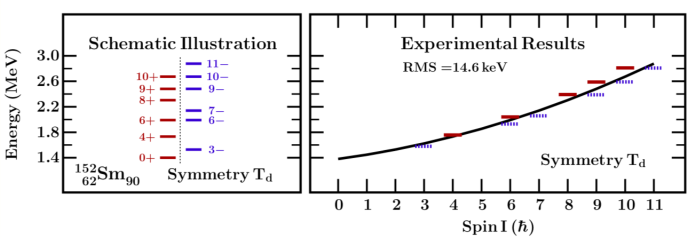

Tetrahedral Band : $I^{\pi}_{T_d} = 0^+, 3^-, 4^+, 6^{\pm}, 7^-, 8^+, 9^{\pm}, 10^{\pm}, 11^-, \ldots$

→ **Published in: J. Dudek et al., PHYSICAL REVIEW C 97, 021302(R) (2018)**

- **Analysing NNDC experimental evidence for ^{152}Sm took 3 months of manual work**

- Rotational band structure of a nucleus in a D_{2d}-symmetry configuration

$D_{2d} \to A_1:$ 0^+,
$2^\pm$,
3^-,
$2\times 4^+,\ 4^-$,
$5^\pm$,
$2\times 6^\pm$,
$7^+,\ 2\times 7^-$,
$3\times 8^+,\ 2\times 8^-$,
$2\times 9^\pm$,
$3\times 10^\pm$,
$2\times 11^+,\ 3\times 11^-$,
$4\times 12^+,\ 3\times 12^-, \ldots$

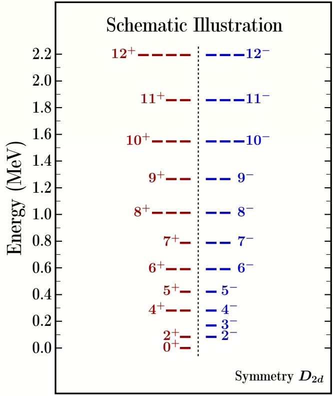

Degeneracy pattern $(\alpha_{20}, \alpha_{32})$

- Rotational band structure of a nucleus in a D_{3h}-symmetry configuration

$D_{3h} \to A_1'$: 0^+,
2^+,
3^-,
$4^\pm$,
5^-,
$2 \times 6^+,\ 6^-$,
$7^\pm$,
$2 \times 8^+,\ 8^-$,
$9^+,\ 2 \times 9^-$,
$2 \times 10^\pm$,
$11^+,\ 2 \times 11^-$,
$3 \times 12^+,\ 2 \times 12^-, \ldots$

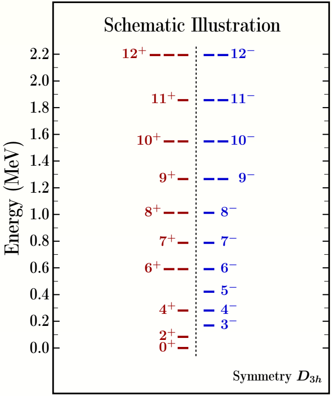

Degeneracy pattern $(\alpha_{20}, \alpha_{33})$

- Rotational band structure of a nucleus in a C_{2v}-symmetric configuration

$C_{2v} \to A_1$:
0^+,
1^-,
$2 \times 2^+,\ 2^-$,
$3^+,\ 2 \times 3^-$,
$3 \times 4^+,\ 2 \times 4^-$,
$2 \times 5^+,\ 3 \times 5^-$,
$4 \times 6^+,\ 3 \times 6^-$,
$3 \times 7^+,\ 4 \times 7^-$,
$5 \times 8^+,\ 4 \times 8^-$,
$4 \times 9^+,\ 5 \times 9^-$,
$6 \times 10^+,\ 5 \times 10^-$,
$5 \times 11^+,\ 6 \times 11^-$,
$7 \times 12^+,\ 6 \times 12^-$, ...

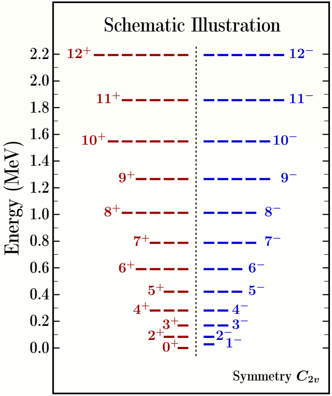

Degeneracy pattern $(\alpha_{20}, \alpha_{31})$

And now . . .

And now . . .

to our knowledge . . .

And now . . .

to our knowledge . . .

the world first experimental evidence

And now . . .

to our knowledge . . .

the world first experimental evidence

of the nuclear C_{2v} symmetry in Actinides

^{234}U and ^{236}U

- Rotational band structure of a nucleus in a C_{2v}-symmetric configuration

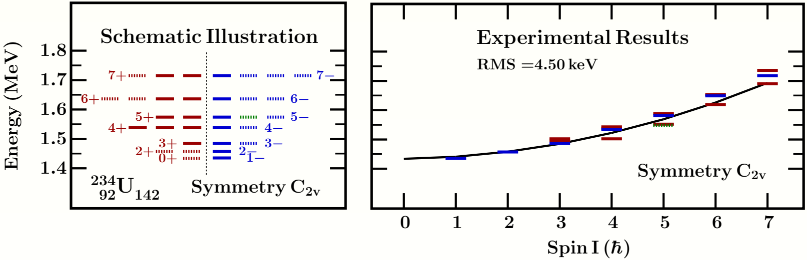

Attention: Experimental degeneracies for ^{234}U according to NNDC

- Rotational band structure of a nucleus in a C_{2v}-symmetric configuration

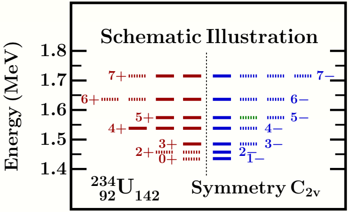

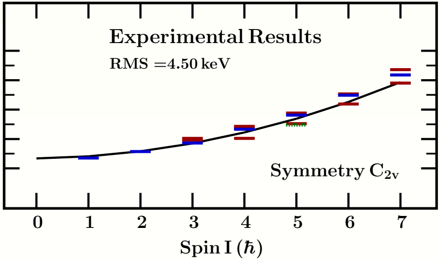

Attention: Experimental degeneracies for ^{234}U according to NNDC

- **Conclusions:**

1) Single rotational band followed by 16 states with rms deviation 4.5 keV

- Rotational band structure of a nucleus in a C_{2v}-symmetric configuration

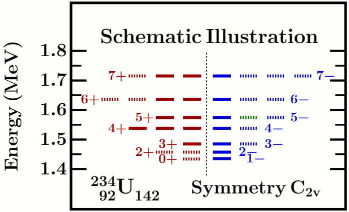

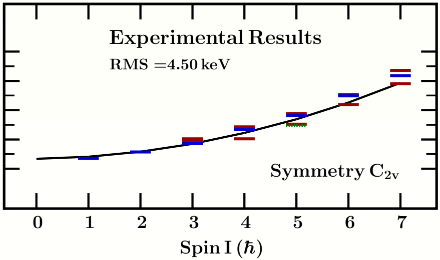

Attention: Experimental degeneracies for ^{234}U according to NNDC

- **Conclusions:**

1) Single rotational band followed by 16 states with rms deviation 4.5 keV

2) Degeneracies characteristic for C_{2v}-symmetry, even if partial, are there

- Rotational band structure of a nucleus in a C_{2v}-symmetric configuration

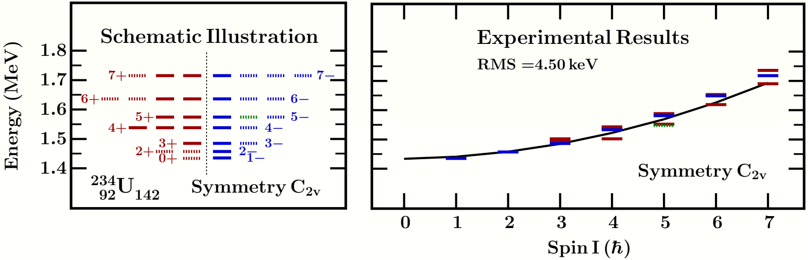

Attention: Experimental degeneracies for ^{234}U according to NNDC

- **Conclusions:**

1) Single rotational band followed by 16 states with rms deviation 4.5 keV

2) Degeneracies characteristic for C_{2v}-symmetry, even if partial, are there

3) Proposals for the new experiments to expand the evidence – called for

- Rotational band structure of a nucleus in a C_{2v}-symmetric configuration

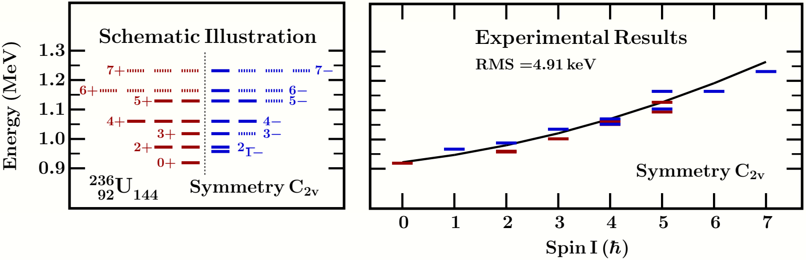

Attention: **Experimental** **degeneracies for ^{236}U according to NNDC**

- Rotational band structure of a nucleus in a C_{2v}-symmetric configuration

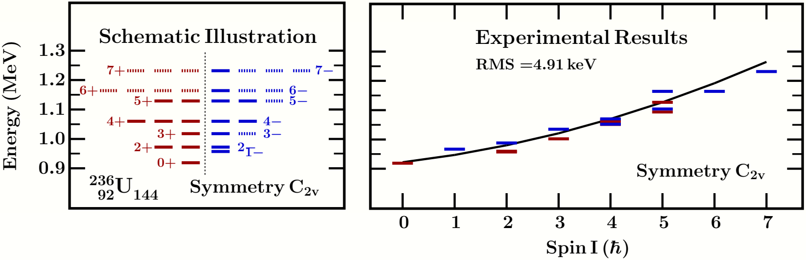

Attention: Experimental degeneracies for ^{236}U according to NNDC

- **Conclusions:**

1) Single rotational band followed by 18 states with rms deviation 4.9 keV

- Rotational band structure of a nucleus in a C_{2v}-symmetric configuration

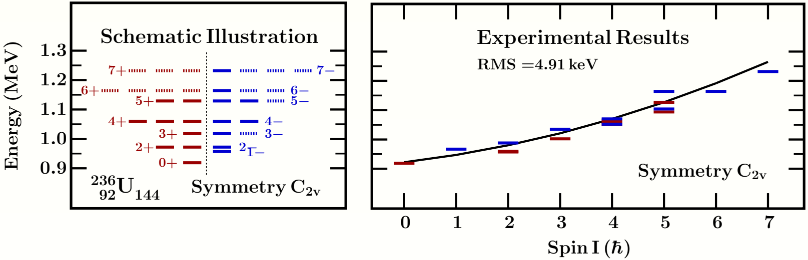

Attention: Experimental degeneracies for ^{236}U according to NNDC

- **Conclusions:**

1) Single rotational band followed by 18 states with rms deviation 4.9 keV

2) Degeneracies characteristic for C_{2v}-symmetry, even if partial, are there

- Rotational band structure of a nucleus in a C_{2v}-symmetric configuration

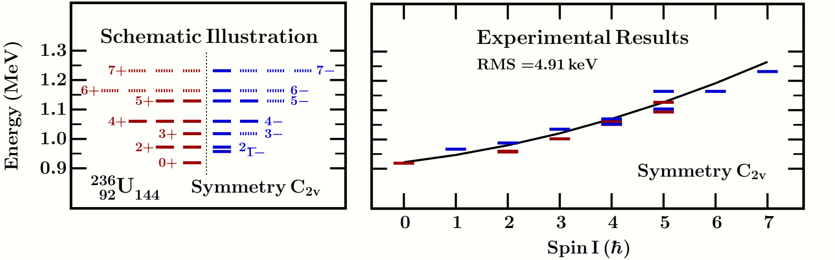

Attention: Experimental degeneracies for ^{236}U according to NNDC

- **Conclusions:**

1) Single rotational band followed by 18 states with rms deviation 4.9 keV

2) Degeneracies characteristic for C_{2v}-symmetry, even if partial, are there

3) Dashed lines represent the missing experimental levels - new proposals?

- **Analysing NNDC experimental data for $\mathrm{T_d}$ symmetry in ^{152}Sm** **took 3 months of manual work**

- **Analysing NNDC experimental data for $\mathbf{T_d}$ symmetry in ^{152}Sm**
  took 3 months of manual work

- **Collecting experimental evidence via NNDC for $\mathbf{C_{2v}}$ in ^{236}U**
  took 30 seconds of computer program*)

***) Collaboration with M. Martin, Simon Fraser University, Canada**

Part V

Large Amplitude Fluctuations:

Dynamical (Most Probable) Deformations and Energy-Doublets as Research Tools

Flat energy landscapes provide a good example of

Ill-defined notion of nuclear equilibrium deformation

*) See next slide: D. Rouvel and J. Dudek, PHYS. REV. C 99, 041303(R) (2019)

Collective Schrödinger Equation Approach

Flat energy landscapes provide a good example of

Ill-defined notion of nuclear equilibrium deformation

- We wish to calculate the most probable deformations resulting from nuclear collective motion following Bohr theory*) ($\{\alpha_{\lambda\mu}\} \to \{q^n\} \leftrightarrow q$)

*) See next slide: D. Rouvel and J. Dudek, PHYS. REV. C 99, 041303(R) (2019)

Collective Schrödinger Equation Approach

Flat energy landscapes provide a good example of

Ill-defined notion of nuclear equilibrium deformation

- We wish to calculate the most probable deformations resulting from nuclear collective motion following Bohr theory*) ($\{\alpha_{\lambda\mu}\} \to \{q^n\} \leftrightarrow q$)

- The corresponding collective Schrödinger equation has the form

$$\hat{H}_{\rm col}\Psi_{{\rm col};i} = E_{{\rm col};i}\Psi_{{\rm col};i},$$

with

$$\hat{H}_{\rm col} = -\frac{\hbar^2}{2}\Delta + V(q).$$

*) See next slide: D. Rouvel and J. Dudek, PHYS. REV. C 99, 041303(R) (2019)

Collective Schrödinger Equation Approach

Flat energy landscapes provide a good example of

Ill-defined notion of nuclear equilibrium deformation

- We wish to calculate the most probable deformations resulting from nuclear collective motion following Bohr theory*) ($\{\alpha_{\lambda\mu}\} \to \{q^n\} \leftrightarrow q$)

- The corresponding collective Schrödinger equation has the form

$$\hat{H}_{\rm col}\Psi_{{\rm col};i} = E_{{\rm col};i}\Psi_{{\rm col};i},$$

with

$$\hat{H}_{\rm col} = -\frac{\hbar^2}{2}\Delta + V(q).$$

- Here, the constant mass is replaced by the mass tensor $B^{nm} = B^{nm}(q)$

$$\Delta = \sum_{m,n=1}^{d} \frac{1}{\sqrt{|B|}}\frac{\partial}{\partial q^n}\left(\sqrt{|B|}B^{nm}\frac{\partial}{\partial q^m}\right),$$

*) See next slide: D. Rouvel and J. Dudek, PHYS. REV. C 99, 041303(R) (2019)

For the Formalism followed – See the Article:

PHYSICAL REVIEW C **99**, 041303(R) (2019)

Rapid Communications

New approach to the adiabaticity concepts in the collective nuclear motion: Impact for the collective-inertia tensor and comparisons with experiment

D. Rouvel[1,2,*] and J. Dudek[2,3,†]

[1]*Lycée Kléber, 25 place de Bordeaux, F-67000 Strasbourg, France*

[2]*IPHC/DRS and Université de Strasbourg, 23 rue du Lœss, B.P. 28, F-67037 Strasbourg Cedex 2, France*

[3]*Institute of Physics, Marie Curie-Skłodowska University, PL-20031 Lublin, Poland*

(Received 5 March 2018; published 19 April 2019)

We propose a new derivation of the cranking-model expression for the nuclear collective inertia tensor, introducing explicitly the slow- and fast-motion timescales together with a parameter controlling the interplay between the two modes. The new cranking formula is free from the mass tensor divergencies originating from the nucleon-level crossings in the denominators of the first-order perturbation theory expressions and allows the exploration of the unrestricted deformation space without spurious mass tensor contributions caused by those divergencies. We apply the new formalism without extra parameter adjustments to the collective vibrations in ^{208}Pb.

DOI: 10.1103/PhysRevC.99.041303

Collective Motion Liberates New Degrees of Freedom

- Most importantly: The mass tensor enters the probability calculus

$$dV \equiv dq^1\, dq^2\, \ldots\, dq^n \qquad <\psi|\hat{\mathcal{O}}|\psi> = \int \psi^* \hat{\mathcal{O}} \psi \sqrt{\det(\mathrm{B(q)})}\, dV$$

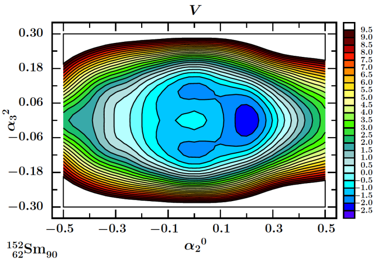

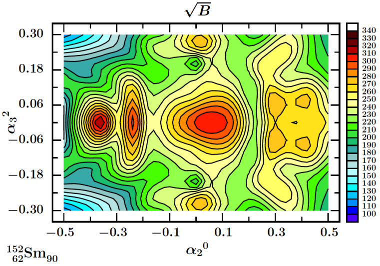

- Observe the space dependence (e.g. maxima and minima) of the term $\sqrt{\det(\mathrm{B(q)})}$ thus influencing the most probable deformations

Another Liberty Contained in Excitation Spectra

$$\hat{H}_{\rm col}\Psi_{{\rm col};i} = E_{{\rm col};i}\Psi_{{\rm col};i}$$

Solution for $i = 1$ | Solution for $i = 2$

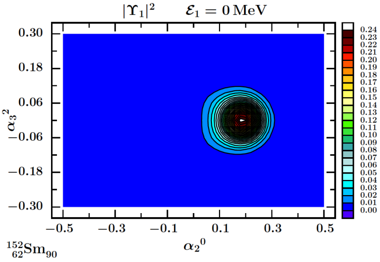

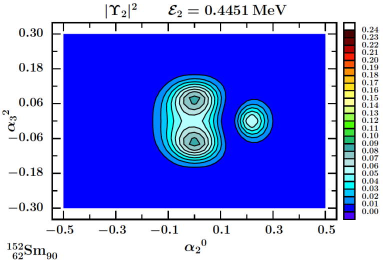

- Observe varying number of maxima and of their relative positions

Another Liberty Contained in Excitation Spectra

$$\boxed{\hat{H}_{\rm col}\Psi_{{\rm col};i} = E_{{\rm col};i}\Psi_{{\rm col};i}}$$

Solution for $i = 2$

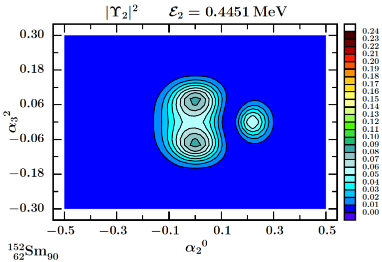

Solution for $i = 3$

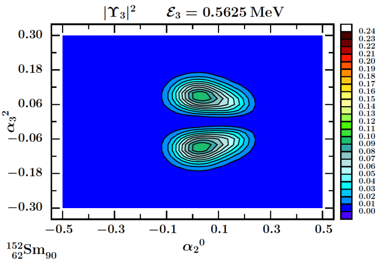

- Observe varying number of maxima and of their relative positions

Another Liberty Contained in Excitation Spectra

$$\hat{H}_{\rm col}\Psi_{{\rm col};i} = E_{{\rm col};i}\Psi_{{\rm col};i}$$

Solution for $i = 3$

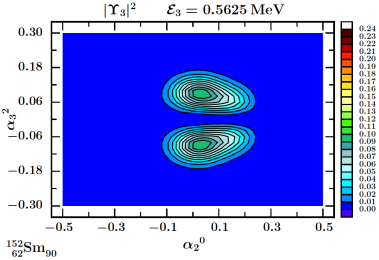

Solution for $i = 4$

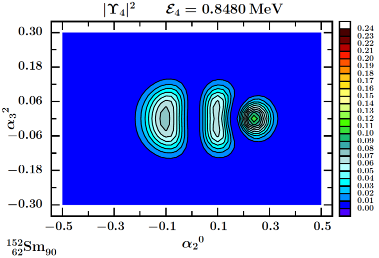

- Observe varying number of maxima and of their relative positions

Another Liberty Contained in Excitation Spectra

$$\hat{H}_{\rm col}\Psi_{{\rm col};i} = E_{{\rm col};i}\Psi_{{\rm col};i}$$

Solution for $i = 4$

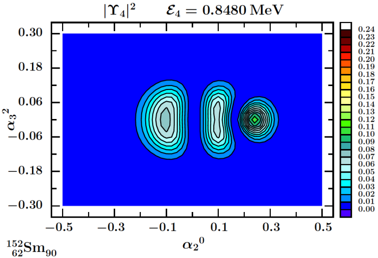

Solution for $i = 5$

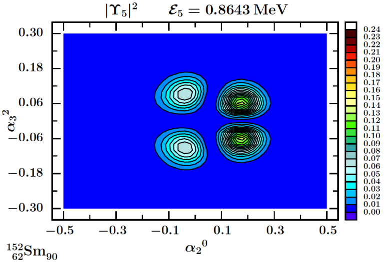

- Observe varying number of maxima and of their relative positions

Illustrations for a Simplified 1D Version

- Solutions of the collective Schrödinger equation can be used to construct criteria of experimental verifications, e.g. energy doublets
- In the present case we will examine characteristic energy doublets
- Behaviour of those doublets depends on the separating barrier V_s
- This mechanism provides rich tools for experimental tests, Ref.*)

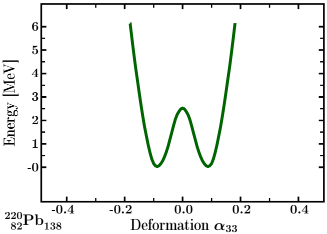

*) Pedagogical discussions in S. C. Pancholi, **"Pear-Shaped Nuclei"** (World Scientific, Singapore, 2020).

Illustrations for a Simplified 1D Version

- We will simplify the illustrations with the help of 1D projections

$$\left[-\frac{\hbar^2}{2}\left(\frac{1}{\sqrt{B(q)}}\frac{d}{dq}\right)\left(\frac{1}{\sqrt{B(q)}}\frac{d}{dq}\right)+V(q)\right]\Psi_i(q)=E_i\Psi_i(q),\ \text{with } q=\alpha_{33},$$

- Introduce an integral measure of the most probable deformation

$$\overline{|\alpha|}_{0,1} \overset{df.}{=} \int \Psi^*_{0,1}(\alpha)|\alpha|\,\Psi_{0,1}(\alpha)\,d\alpha \to \langle\alpha^2\rangle_{0,1} \overset{df.}{=} \int \Psi^*_{0,1}(\alpha)\alpha^2\,\Psi_{0,1}(\alpha)\,d\alpha,$$

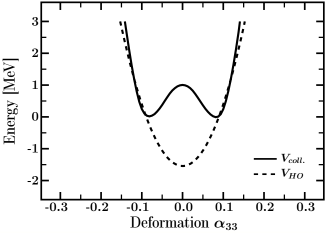

- It turns out that the two measures of dynamical deformation are close and

$$\boxed{\overline{|\alpha|}_{0,1} < \sqrt{\langle\alpha^2\rangle}_{0,1}}$$

Illustration of the Role of the Average Inertia: Part 1

• We set $B(q) \to \overline{B(q)} \leftrightarrow B_{\rm Mass}$ and adjust it to examine the effect of varying eigen-energies vs. top of the barrier, to begin with $E_0 \sim (1/2)V_B$

$$\left[-\frac{\hbar^2}{2}\left(\frac{1}{\sqrt{B(q)}}\frac{d}{dq}\right)\left(\frac{1}{\sqrt{B(q)}}\frac{d}{dq}\right)+V(q)\right]\Psi_i(q)=E_i\Psi_i(q), \text{ with } q=\alpha_{33},$$

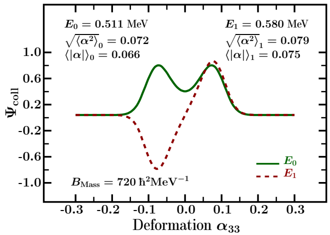

• Notice: $\{E_0, \psi_0\}$ corresponds to $\boxed{\pi = +}$ and $\{E_1, \psi_1\}$ to $\boxed{\pi = -}$

• The two solutions with $E_0 = 0.51$ MeV and $E_1 = 0.58$ MeV are nearly degenerate $\to$ Characteristic, nearly degenerate collective vibrational states

Illustration of the Role of the Average Inertia: Part 2

- We proceed decreasing the average mass value to approach $E_0 \sim V_B$

$$\left[-\frac{\hbar^2}{2}\left(\frac{1}{\sqrt{B(q)}}\frac{d}{dq}\right)\left(\frac{1}{\sqrt{B(q)}}\frac{d}{dq}\right)+V(q)\right]\Psi_i(q)=E_i\Psi_i(q),\ \text{with}\ q=\alpha_{33},$$

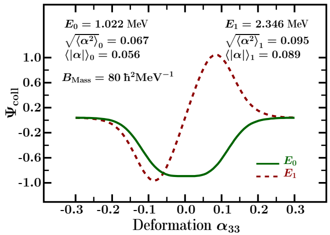

- Notice: $\{E_0, \psi_0\}$ corresponds to $\boxed{\pi = +}$ and $\{E_1, \psi_1\}$ to $\boxed{\pi = -}$

- The two solutions with $E_0 = 1.02$ MeV and $E_1 = 2.34$ MeV are incomparable, E_2 more than double of the ground-state value $\rightarrow$ A clear difference

Such varying differences can help interpreting experimental results

Illustration of the Role of the Average Inertia: Part 3

- We proceed decreasing the average mass value to approach $E_0 \sim 2 \times V_B$

$$\left[-\frac{\hbar^2}{2}\left(\frac{1}{\sqrt{B(q)}}\frac{d}{dq}\right)\left(\frac{1}{\sqrt{B(q)}}\frac{d}{dq}\right)+V(q)\right]\Psi_i(q)=E_i\Psi_i(q),\ \text{with}\ q=\alpha_{33},$$

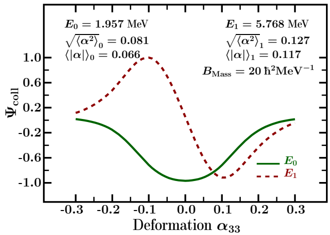

- Notice: $\{E_0, \psi_0\}$ corresponds to $\boxed{\pi = +}$ and $\{E_1, \psi_1\}$ to $\boxed{\pi = -}$
- The two solutions $E_0 = 1.96$ MeV and $E_1 = 5.74$ MeV differ still stronger

Such varying differences can help interpreting experimental results

PHYSICAL REVIEW C **107**, 054304 (2023)

Islands of oblate hyperdeformed and superdeformed superheavy nuclei with D_{3h} point group symmetry in competition with normal-deformed D_{3h} states: "Archipelago" of D_{3h}-symmetry islands

J. Yang,[1,2] J. Dudek,[3,*] I. Dedes,[4] A. Baran,[2] D. Curien,[3] A. Gaamouci,[4] A. Góźdź,[2] A. Pędrak,[5] D. Rouvel,[3] and H. L. Wang[1]

[1]*School of Physics and Microelectronics, Zhengzhou University, Zhengzhou 450001, China*
[2]*Institute of Physics, Marie Curie-Skłodowska University, PL-20 031 Lublin, Poland*
[3]*Université de Strasbourg, CNRS, IPHC UMR 7178, F-67 000 Strasbourg, France*
[4]*Institute of Nuclear Physics Polish Academy of Sciences, PL-31 342 Kraków, Poland*
[5]*National Centre for Nuclear Research, Theoretical Physics Division, Pl-02-093 Warsaw, Poland*

(Received 4 October 2022; revised 26 March 2023; accepted 7 April 2023; published 10 May 2023)

In two recent articles we have formulated nuclear mean-field theory predictions of existence of a new form of magic numbers, referred to as fourfold magic numbers. These predictions stipulate the presence of strong shell closures at the neutron numbers $N = 136$ (actinide region) and $N = 196$ (superheavy region) simultaneously at nonvanishing all four octupole deformations $\alpha_{3\mu=0,1,2,3} \neq 0$. In contrast to the traditional notion of magic numbers, the new notion refers to simultaneous nonspherical configurations ($\alpha_{3\mu} \neq 0$, $\alpha_{2\mu} = 0$). In this article we study the nuclear equilibrium deformations with $\alpha_{33} \neq 0$ combined with nonvanishing quadrupole deformation, $\alpha_{20} \neq 0$. One easily shows that such geometrical shapes have a threefold symmetry axis and are invariant under the symmetry operations of the D_{3h} point group. We employ a realistic phenomenological mean-field approach with the so-called universal deformed Woods-Saxon potential and its recently optimized parametrization based on actualized experimental data with the help of the *inverse problem theory* methods. The presence of parametric correlations among 4 of 12 parameters in total was detected and removed employing Monte Carlo approach leading to stabilization of the modeling predictions. Our calculations predict the presence of three nonoverlapping groups of nuclei with D_{3h} symmetry, referred to as islands on the nuclear (Z, N) plane (mass table). These islands lie in the rectangle $110 \leqslant Z \leqslant 138$ and $166 \leqslant N \leqslant 206$. The "repetitive" structures with the D_{3h} symmetry minima are grouped in three zones of oblate quadrupole deformation, approximately, at $\alpha_{20} \in [-0.10, -0.20]$ (oblate normal deformed), around $\alpha_{20} \approx -0.5$ (oblate superdeformed) and $\alpha_{20} \approx -0.85$ (oblate hyperdeformed). Importantly, the energies of those latter exotic deformation minima are predicted to be very close to the ground-state energies. We illustrate, compare, and discuss the evolution of the underlying shell structures. Nuclear surfaces parametrized as usual with the help of *real* deformation parameters, $\{\alpha_{\lambda\mu} = \alpha^*_{\lambda\mu}\}$,

Basing on this article a few illustrations for super-heavy nuclei will follow

Collective Solutions for a Normal Oblate Shape

- Below the mass tensor was calculated microscopically (new method)

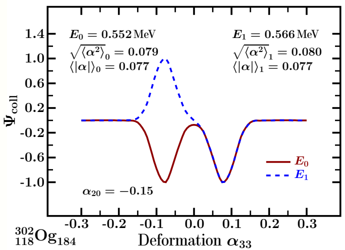

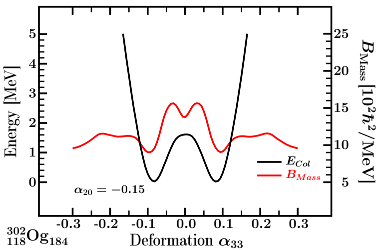

- The result of energy doublet $E_0 = 0.55$ MeV and $E_1 = 0.57$ MeV can be seen as a realistic prediction from realistic mean field theory

If we can populate such a nucleus we should expect those doublets

Illustrations for a Super-deformed Oblate Shape

- Below the mass tensor was calculated microscopically (new method)

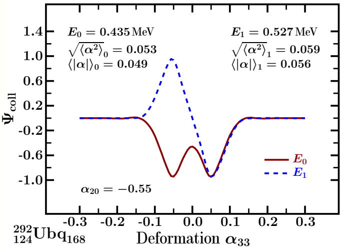

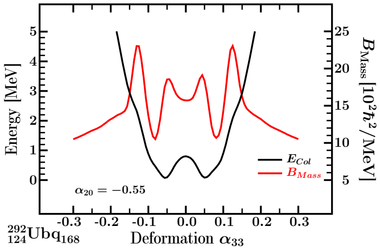

- The result of parity doublet $E_0 = 0.44$ MeV and $E_1 = 0.53$ MeV can be seen as a realistic prediction from realistic mean field theory

If we can populate such a nucleus we should expect these doublets

Illustrations for a Hyper-deformed Oblate Shape

- Below the mass tensor was calculated microscopically (new method)

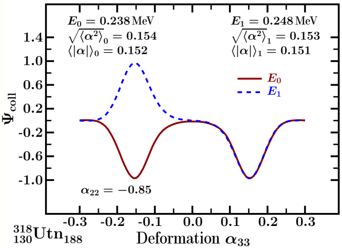

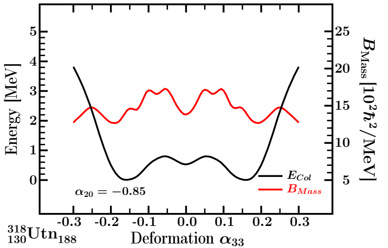

- The result of parity doublet $E_0 = 0.24$ MeV and $E_1 = 0.25$ MeV can be seen as a realistic prediction from realistic mean field theory

If we can populate such a nucleus we should expect these doublets

Short Summary of This Part of the Discussion

• We have developed new formulation of the adiabaticity approach to microscopic modelling of the nuclear collective inertia & tensor

• Collective vibrational excitations in ^{208}Pb were reproduced without parameter adjustments

• Collective inertia impacts the nuclear deformation probability

• These are those most probable (dynamical) equilibrium deformations which should be compared with experiment rather than static deformation points

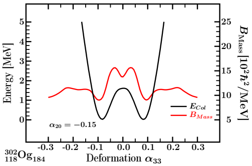

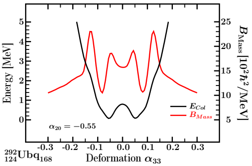

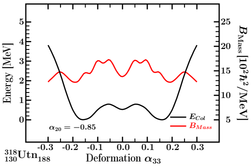

Part VI

Summary: First Time Predictions & Challenges

• Systematic study of **molecular symmetries in** heavy and super-heavy **nuclei** $\leftarrow$ realistic phenomenological mean field Hamiltonian

• Modern Hamiltonian-optimisation using **inverse problem theory**

• Systematic derivation of the **experimental identification** rules of **molecular symmetries** in nuclei with new rotational band properties

• Nuclear spectroscopy challenges $\leftrightarrow$ **Multiple level-degeneracies**

• Discovery $\rightarrow$ **first experimental evidence** of nuclear $\boldsymbol{T_{\mathbf{d}}}$ and $\boldsymbol{C_{\mathbf{2v}}}$ symmetries – systematic predictions for heavy / super-heavy nuclei

• Large amplitude motion within **new formulation of Bohr theory:**
– **New formulation of nuclear adiabaticity principles**
– New calculation techniques for the **nuclear inertia tensor**
– New technique for **dynamical** vs. static **equilibrium deformations**